

GAS BITUMEN COLD LAKE HEARING

UNDERTAKINGS GIVEN BY HUSKY

Undertaking No. 1

To provide graphs showing the relative permeability curves Husky used in its model runs, including any adjustments it made to the curves such as temperature adjustments.

Undertaking No. 2

To advise if the input and output files that were submitted by Husky have the same convergence criteria as those used in the runs provided with its January 30th reply evidence and that those are not the same as the default criteria.

Undertaking No. 3

To advise how the 20 percent porosity and 50 percent water saturation correlates to bitumen weight percent.

Undertaking No. 4

To file the Reynolds paper and the relevant page referenced.

Undertaking No. 5

To provide the variograms developed by facies for porosity and water saturation.

Undertaking No. 6

To produce the logs for the 6-34 and the 7-19 Well.

Undertaking No. 7

To explain the lack of a neutron response on said log with respect to the 7-19 Well.

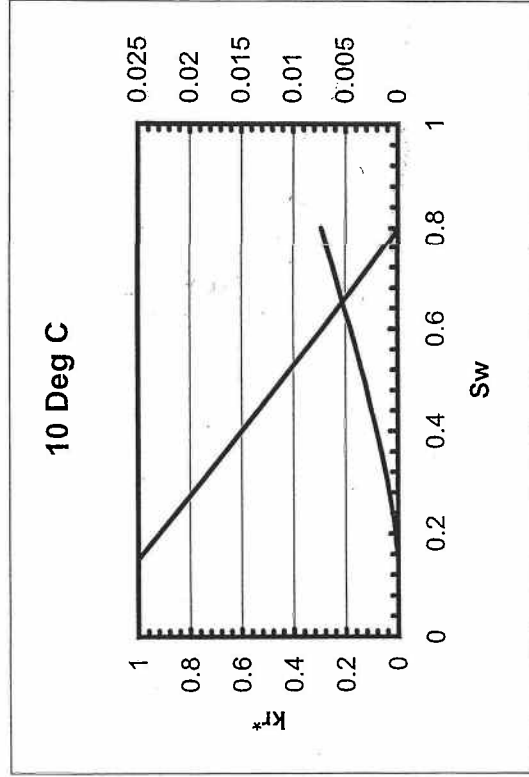
Undertaking No. 1

FROM THE HUSKY SIMULATION .OUT FILE

*** DATA AT TEMPERATURE OF 10.00 C ***

--- WATER-OIL SYSTEM ---

	Sw	Krw	Krow	Pcow
0.15	1	0	0	0
0.1882	0.9383	0.0002	0	0
0.2265	0.8768	0.0004	0	0
0.2647	0.8156	0.0007	0	0
0.3029	0.7545	0.001	0	0
0.3412	0.6937	0.0014	0	0
0.3794	0.6331	0.0018	0	0
0.4176	0.5728	0.0022	0	0
0.4559	0.5128	0.0027	0	0
0.4941	0.4532	0.0031	0	0
0.5324	0.3939	0.0036	0	0
0.5706	0.335	0.0041	0	0
0.6088	0.2767	0.0046	0	0
0.6471	0.2189	0.0052	0	0
0.6853	0.1618	0.0057	0	0
0.7235	0.1057	0.0062	0	0
0.7618	0.0511	0.0068	0	0
0.8	0	0.0074	0	0





Husky Caribou SAGD and CSS Core Displacement Testing

Well 1AA/03-07-069-04 W4M - 40% Clay Content Core, 489-492 m Interval

Summary of Core and Test Parameters

Parameter	Value	Unit
Core ID	12A/03-07-069-04 W4M	
Core Length	4.90	m
Core Diameter	76.25	mm
Core Weight	3.46	kg
Core Volume	9.38	cm ³
Core Pore Volume	1.02	cm ³
Core Permeability	2.38	md
Core Porosity	9.91	%
Core Saturation	80.00	%
Core Temperature	230.00	deg C
Core Pressure	20.00	MPa
Core Location	489-492 m	
Core Description	Simulated Formation Brine (15,000 ppm NaCl)	
Core Fluid	Fresh Water	

Fluid Viscosity Data

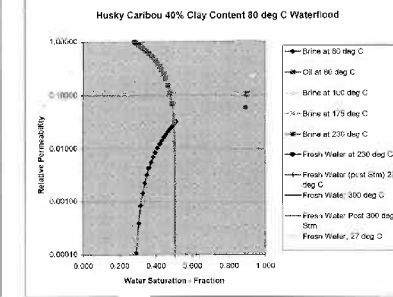
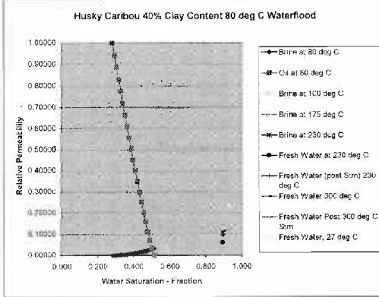
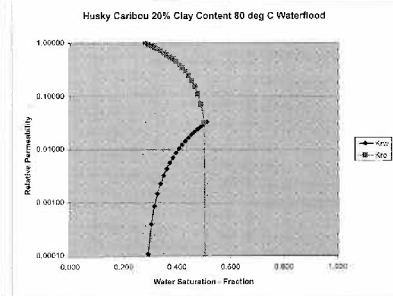
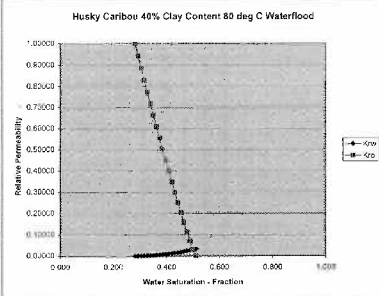
Fluid	Temperature (deg C)	Viscosity (cp)
Clearwater	80	0.035
Formation Brine	80	0.355
Formation Brine	100	0.242
Formation Brine	175	0.115
Formation Brine	230	0.118
Fresh Water	80	0.114
Fresh Water	100	0.088
Fresh Water	175	0.049

Permeability and Saturation Summary

Displacing Fluid	Test Temperature (deg C)	Permeability (mD)	Relative Permeability	Saturation Oil Fraction	Saturation Water Fraction	Saturation Gas Fraction	% Res CO ₂
Clearwater	80	3187	1.0000	0.228	0.772	0.000	0.00%
Formation Brine	80	102	0.0324	0.468	0.532	0.000	0.00%
Formation Brine	100	132.4	0.0427	0.418	0.582	0.000	44.6%
Formation Brine	175	207.2	0.0657	0.327	0.673	0.000	83.9%
Formation Brine	230	346.5	0.1081	0.177	0.823	0.000	82.1%
Fresh Water	80	1.0	0.0003	0.407	0.593	0.000	85.1%
Fresh Water (post Sorb)	230	1.0	0.0003	0.102	0.898	0.000	86.4%
Fresh Water	230	39.8	0.1255	0.308	0.692	0.000	85.4%
Fresh Water	300	305.8	0.1144	0.106	0.894	0.000	86.1%
Fresh Water (post Sorb)	300	366.2	0.1162	0.072	0.928	0.000	90.6%
Fresh Water	27	1.0	0.0003	0.372	0.628	0.000	80.6%

Water-Oil Relative Permeability Data at 80 deg C

Water Saturation - Frcn	K _{rw}	K _{ro}
0.792	0.01339	1.00000
0.729	0.00111	0.94000
0.666	0.00038	0.88600
0.603	0.00004	0.83200
0.540	0.00000	0.77800
0.477	0.00000	0.72400
0.414	0.00000	0.67000
0.351	0.00000	0.61600
0.288	0.00000	0.56200
0.225	0.00000	0.50800
0.162	0.00000	0.45400
0.100	0.00000	0.40000
0.037	0.00000	0.34600
0.000	0.00000	0.29200
0.000	0.00000	0.23800
0.000	0.00000	0.18400
0.000	0.00000	0.13000
0.000	0.00000	0.07600
0.000	0.00000	0.02200
0.000	0.00000	0.00000





Husky Caribou SAGD and CSS Core Displacement Testing

Well 1AA/03-07-069-04 W4M - 20% Clay Content Core, 471-475 m Interval

Summary of Core and Test Parameters

Field Location	Corewell	Corewell
Well Location	1AA/03-07-069-04 W4M	
Depth	471 - 475	meters
Formation	Clearwater Sandstone	
Block Length	28.72	cm
Core Diameter	3.45	cm
Block Area	9.35	cm ²
Block Pore Volume	268.83	cm ³
Block Permeability	0.08	md-ft
Spore Pore Volume	192.24	cm ³
Permeability Factor	80.25	md-ft
Water Permeability	2000	md-ft
Core Disposition Pressure	450	psi
Displacement Fluid #1	Corewell Oil (20% Clay Oil)	1 - 100%
Displacement Fluid #2	Simulated Formation Brine (10,000 ppm NaCl)	1 - 100%
Displacement Fluid #3	Fresh Water	1 - 100%

Fluid Viscosity Data

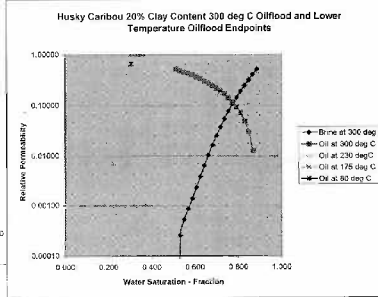
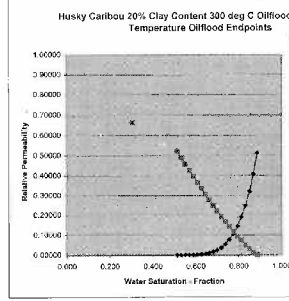
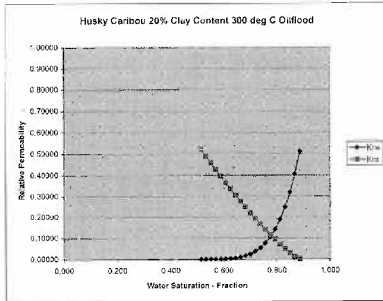
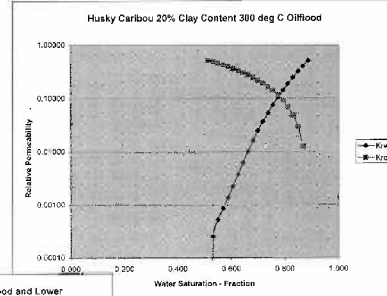
Fluid	Temperature (°C)	Viscosity (cP)
Corewell Oil at 175	80	454.0
Corewell Oil at 175	100	225.0
Corewell Oil at 175	125	214
Corewell Oil at 175	200	82
Corewell Oil at 175	280	2
Corewell Oil at 175	300	0.997
Fresh Water	300	0.076

Permeability and Saturation Summary

Displacing Fluid	Test Temperature (°C)	Permeability (md)	Relative Permeability	Shrinkage - Oil (%)	Saturation - Water (%)	Saturation - Gas (%)	% Rec. OOIP
Corewell Oil at 175	80	0.08	0.000	0.000	0.000	0.000	0%
Corewell Oil at 175	100	1511.3	0.990	0.777	0.000	0.000	0%
Corewell Oil at 175	125	738.3	0.186	0.515	0.000	0.000	56.9%
Corewell Oil at 175	200	473.3	0.202	0.412	0.000	0.000	58.8%
Corewell Oil at 175	300	0.08	0.000	0.113	0.887	0.000	85.5%
Fresh Water	300	1633.0	0.133	0.832	0.000	0.000	84.2%
Simulated Formation Brine	300	1691.5	0.186	0.696	0.000	0.000	82.3%
Corewell Oil at 175	220	2100.1	0.875	0.888	0.000	0.000	28.9%
Corewell Oil at 175	175	1633.0	0.186	0.625	0.000	0.000	16.6%
Corewell Oil at 175	80	7376	0.020	0.694	0.926	0.000	10.7%

Oil-Water Relative Permeability Data at 300 deg C

Water Saturation - Fract	K _{rw}	K _{ro}
0.000	0.00000	0.60000
0.005	0.00000	0.60000
0.010	0.00000	0.60000
0.015	0.00000	0.60000
0.020	0.00000	0.60000
0.025	0.00000	0.60000
0.030	0.00000	0.60000
0.035	0.00000	0.60000
0.040	0.00000	0.60000
0.045	0.00000	0.60000
0.050	0.00000	0.60000
0.055	0.00000	0.60000
0.060	0.00000	0.60000
0.065	0.00000	0.60000
0.070	0.00000	0.60000
0.075	0.00000	0.60000
0.080	0.00000	0.60000
0.085	0.00000	0.60000
0.090	0.00000	0.60000
0.095	0.00000	0.60000
1.000	0.00000	0.00000



Undertaking No. 2

Undertaking No. 3

Bulk Weight Oil Calculation for $\Phi = 0.2$, $S_w = 0.5$:

$$\text{Bulk Weight Oil} = \text{weight oil} / [\text{weight oil} + \text{weight water} + \text{weight rock}]$$

Where:

$$\text{Weight oil} = \rho_{\text{oil}} * (1 - S_w) * \Phi$$

$$\text{Weight water} = \rho_w * S_w * \Phi$$

$$\text{Weight rock} = \rho_r * (1 - \Phi)$$

$$\rho_{\text{oil}} = \text{Oil Density} = 0.987 \text{ (EnCana average, Exhibit C28, p. 12)}$$

$$\rho_w = \text{Water Density} = 1.006 \text{ (EnCana average, Exhibit C28, p. 12)}$$

$$\rho_r = \text{rock density} = 2.62 \text{ (see Note below)}$$

$$S_w = \text{water saturation} = 0.50$$

$$\Phi = \text{porosity} = 0.20$$

$$\text{Bulk Weight Oil} = 0.043 \text{ or } 4.3\%$$

Note: The Grain density of 2.62 represents the arithmetic average of Husky Clearwater core analysis grain density values for the 2005 and 2006 core data previously submitted to these proceedings.

Undertaking No. 4

GEOSTATISTICAL RESERVOIR MODELING

Clayton V. Deutsch

APPLIED GEOSTATISTICS SERIES

General Editor
André G. Journel

Clayton V. Deutsch, *Geostatistical Reservoir Modeling*

Jean-Laurent Mallet, *Geomodelling*

Pierre Goovaerts, *Geostatistics for Natural Resources Evaluation*

Clayton V. Deutsch and André G. Journel, *GSLIB: Geostatistical Software
Library and User's Guide, Second Edition*

Edward H. Isaak and R. Mohan Srivastava, *An Introduction to Applied
Geostatistics*

OXFORD
UNIVERSITY PRESS

2002

ograms presented in Figure 4.13, we see evidence of all the behaviors: nugget effect, geometric anisotropy and zonal anisotropy, a vertical trend in the middle example, and cyclicity most pronounced on the bottom image.

Figure 4.14 shows eight vertical normal scores variograms of well log porosity from eight different layers in a reservoir. The variogram for layer 4 appears classical in the sense that it shows a low nugget effect and rises to the theoretical sill of 1.0. All other cases show combinations of cyclicity (layers 1 and 8), vertical trend (layers 2 and 7), and areal trends (layers 3, 5, and 6). Figure 4.15 shows well log data from 3 layers illustrating cyclicity, vertical trend, and an areal trend.

More examples are shown after the section on variogram modeling.

4.4 Horizontal Variograms

Geostatistical reservoir modeling faces a unique problem. Most wells (particularly exploration wells) are vertical. This makes it straightforward to infer the vertical variogram, but difficult to infer a reliable horizontal variogram. Given the overwhelming noise content in sample horizontal variograms, one evident error is to adopt a pure nugget model, which appears to closely fit the experimental variogram values. This is a convenient, but unrealistic, alternative. Our goal is to infer the best parameters for the underlying phenomenon; it is not to obtain a best fit to unreliable experimental statistics. We must consider secondary information in the form of horizontal wells, seismic data, conceptual geological models, and analogue data. In all cases, however, expert judgment is needed to integrate global information from analogue data with sparse local data.

In presence of sparse horizontal data, there are two critical steps to synthesize a horizontal variogram:

1. Determine what fraction of the variance may be explained by zonal anisotropy, that is, stratification that leads to persistent positive correlation in the horizontal direction.
2. Establish the horizontal-to-vertical anisotropy ratio based on secondary data; the synthetic horizontal variogram consists of the zonal anisotropy (step one) and the scaled vertical variogram.

Figure 4.16 shows a schematic illustration of these two parameters. Both the zonal anisotropy contribution and the horizontal-to-vertical anisotropy ratio will have considerable uncertainty. A sensitivity study should be performed in a subsequent geostatistical simulation.

Zonal Anisotropy

There may be persistent stratification that would make the horizontal variogram to plateau different than the sill variance, that is, show zonal anisotropy.

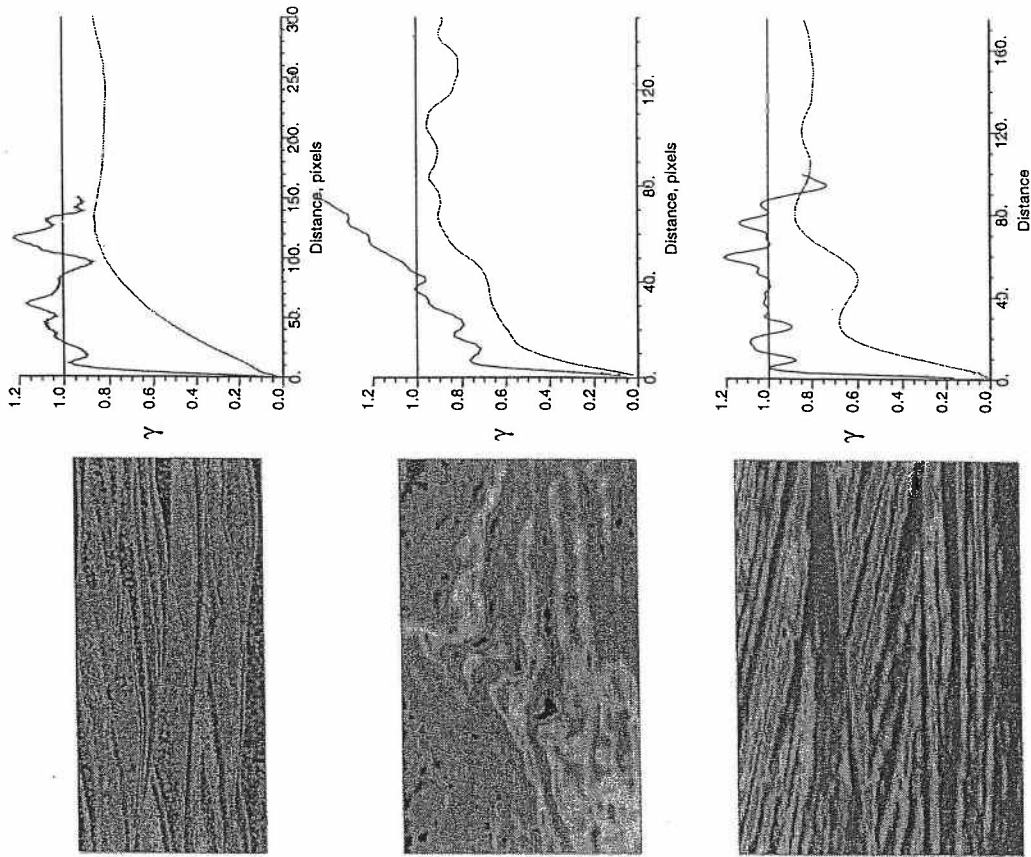


Figure 4.13: Three different geologic images with the corresponding directional variograms. Note the cyclicity, trends, geometric anisotropy, and zonal anisotropy. The top image is an example of migrating ripples in a man-made aeolian sandstone (from the U.S. Wind Tunnel Laboratory), the central image is an example of convoluted and deformed laminations from a fluvial environment. The original core photograph was taken from page 131 of Sandstone Depositional Environments, Scholle and Spearing, 1982. The bottom image is a real example of large-scale cross laminations from a deltaic environment. The original photograph was copied from page 162 of Sandstone Depositional Environments, Scholle and Spearing, 1982.

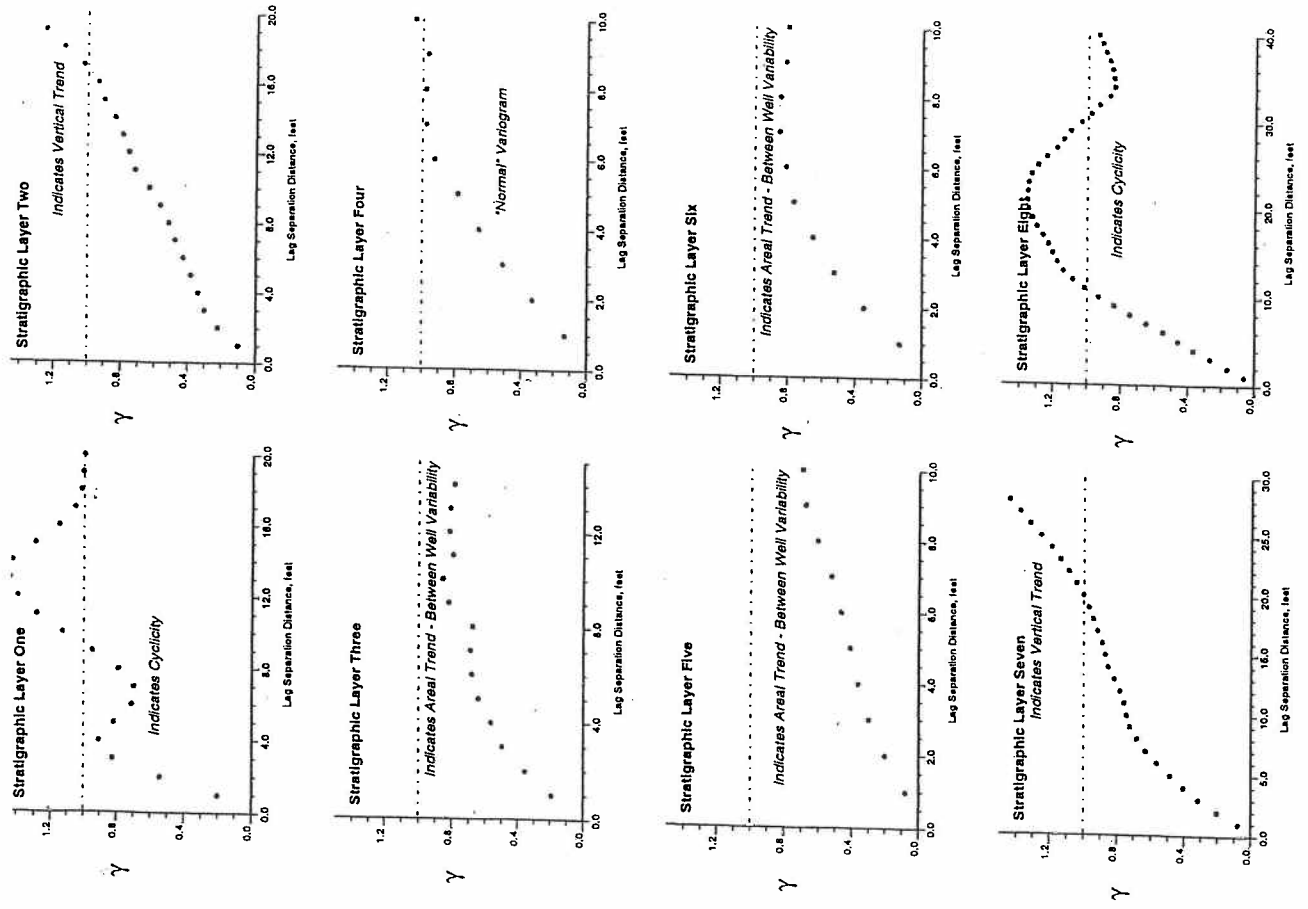


Figure 4.14: Eight variograms, of the normal score transform of porosity, for eight different stratigraphic layers within the same reservoir.

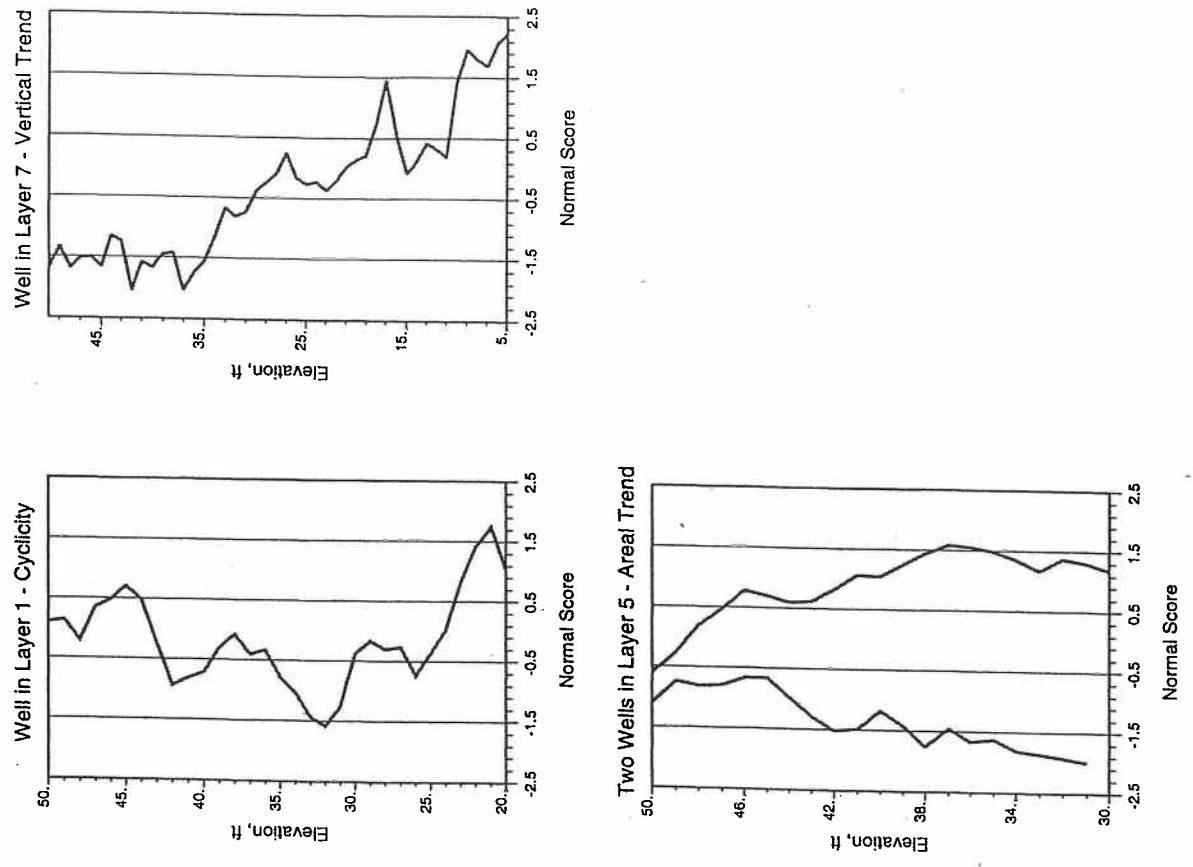


Figure 4.15: Well log data from three layers illustrating cyclicity, vertical trend, and an areal trend.

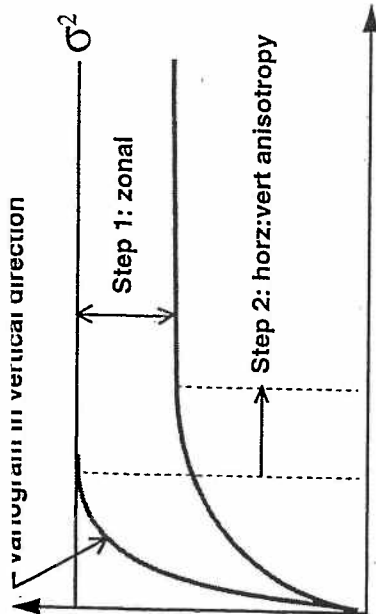


Figure 4.16: Schematic illustration of the two decisions required for horizontal variogram inference in presence of sparse data: (1) the amount of zonal anisotropy, and (2) the horizontal-to-vertical anisotropy ratio.

In presence of sufficient data, this could be observed on directional variograms. In presence of sparse data, that zonal anisotropy must be inferred either from the available well data or from a conceptual geologic model.

A *conceptual geologic model* is essentially an expert opinion or judgment regarding the spatial variability. No reservoir stands in complete isolation. There may be reservoirs in the same sedimentary basin, reservoirs of similar type in different parts of the world, or modern analogues that give some indication of patterns of spatial variation. The "zonal anisotropy" considered here is a specification of the fraction of the variability explained by reservoir-wide stratification. Normally, this is between 0 to 30% of the total variability.

The *available data* may be too few and too widely spaced to calculate a reliable horizontal variogram. Nevertheless, zonal anisotropy consists of reservoir-wide patterns of variation and may be observed with as few as two wells. A horizontal h-scatterplot of values paired at the same stratigraphic vertical coordinate can be constructed; the correlation coefficient is an estimate of the relative magnitude of the zonal anisotropy; a large correlation coefficient indicates a large zonal anisotropy. A correlation coefficient of zero would indicate no zonal anisotropy. This value cannot be used blindly. Outliers or insufficient data would be reason to discredit this approach. Figure 4.17 shows an example with two vertical wells.

Horizontal-to-Vertical Anisotropy Ratio

A horizontal variogram model could consist of the vertical variogram points scaled (1) to show the correct plateau, determined previously, and (2) to show the correct distance scale. The distance scale is determined by establishing a horizontal-to-vertical anisotropy ratio. Secondary information such as hor-

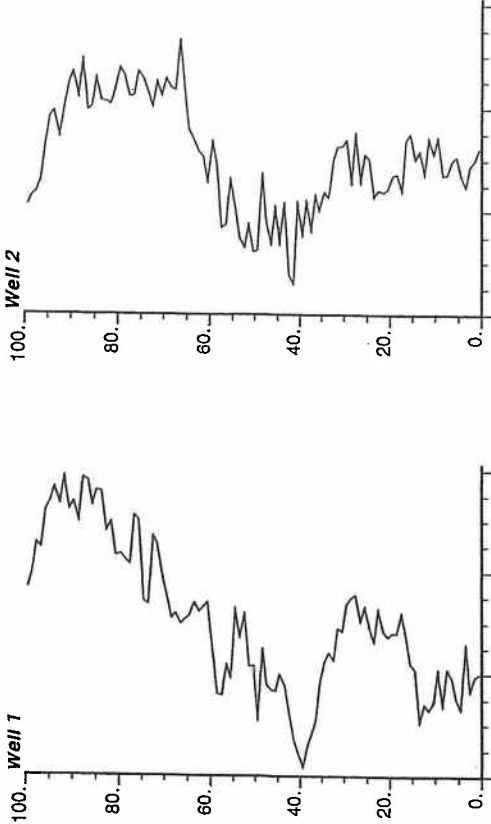


Figure 4.17: Porosity values at two vertical wells and a cross plot of the matching (same stratigraphic position) porosity values from one well to the other.

izontal wells, seismic data, conceptual geological models, and analogue data are considered to establish the required anisotropy ratio.

The increasing popularity of horizontal wells has not significantly helped with horizontal variogram inference. Horizontal wells rarely track the stratigraphic "time lines" or stratigraphic coordinates described in Chapter 3. When wells are close to "stratigraphic" horizontal, experimental horizontal variograms should be calculated. Note that even small departures from horizontal can lead to drastically reduced correlation, that is, an underestimation of the horizontal continuity.

Seismic does not directly measure the facies, porosity, or permeability variables being considered in variogram analysis. Nevertheless, the acoustic responses of seismic are related to these petrophysical properties. One could consider the seismic data as a non-linear average of the underlying petrophysical variables with additional error. The volume-scale difference leads to predictable changes to the variogram behavior if the averaging is linear (see Chapter 11); the range of correlation is increased by the scale of averaging. This is very important for the vertical variogram since the vertical scale of averaging is often many times larger than the vertical range. The large-scale nature of seismic is not as critical in the horizontal direction since the horizontal range of correlation is many times larger than the horizontal scale of averaging. The idea, then, is to use the horizontal range of correlation from seismic.

The extensive lateral coverage of seismic permits calculation of a clear and easy-to-interpret horizontal variogram and horizontal range of correlation. The horizontal-to-vertical anisotropy ratio is calculated from the horizontal seismic variogram and the vertical variogram for the variable being studied.

Conceptual geological models consist of an expert opinion regarding the depositional system and the consequent spatial correlation. Such conceptual models are usually based on analogue data, which may come from (1) other, more extensively sampled, reservoirs, (2) geological process simulation, or (3) outcrop measurements. In all cases, expert judgment is needed to integrate global information from analogues with sparse local data. There are published sources of such data, for example, the compilation of Kupfersberger and Deutsch [167].

Geological-based process models simulate physical processes such as sediment transport, deposition, and erosion to characterize property variations over the time scale in which a reservoir evolved. Such process models are not yet viable reservoir modeling tools; however, we expect them to show the general character of reservoir heterogeneity [50, 262]. Essential features such as the existence of preferential flowpaths or sedimentological organization may be revealed [11]. Geological process models are constrained by the geological variables that create the stratigraphic record such as amount and type of sediment supply. Even if the observed location and geometry of facies units cannot be reproduced exactly, the general character may be appropriate for purposes of horizontal variogram inference [213]. They could be used to construct a "training image" from which horizontal variograms are extracted. This would require significant effort.

Experimental variograms are calculated. Analogue data may be considered to supplement inadequate data. These variograms must be consistent with the geological model of the reservoir. Lastly, the variograms must be modeled.

horizontal:vertical anisotropy

10:1 100:1 1000:1

Point Bars

Braided Fluvial

Eolian

Estuarine

Deepwater

Deltaic

Platform Carbonates

Figure 4.18: Some typical horizontal-to-vertical anisotropy ratio *conceptualized* from available literature and experience. Such generalizations can be used to verify actual calculations and supplement very sparse data.

4.5 Variogram Modeling

The experimental variogram points are not used directly in subsequent geostatistical steps such as kriging and simulation; a parametric variogram model is fitted to the experimental points. There are two reasons why experimental variograms must be modeled:

1. The variogram function is required for all distance and direction vectors h within the search neighborhood of subsequent geostatistical calculations; however, we only calculate the variogram for specific distance lags and directions (often, only along the principal directions of continuity). There is a need to interpolate the variogram function for h values where too few or no experimental data pairs are available. In particular, the variogram is often calculated in the horizontal and vertical directions, but geostatistical simulation programs require the variogram in off-diagonal directions where the distance vector simultaneously contains contributions from the horizontal and vertical directions.
2. The variogram measure $-\gamma(h)$ must have the mathematical property of "positive definiteness" for the corresponding covariance model, that is, we must be able to use the variogram and its covariance counterpart in kriging and stochastic simulation. A positive definite model ensures that the kriging equations can be solved and that the kriging variance is positive.

Dimensions of Paralic Sandstone Bodies¹

A. D. Reynolds²

ABSTRACT

Petroleum reservoirs in paralic successions commonly comprise a wide range of sand-body types. To estimate the volume of petroleum that is present and the percentage that is recoverable, and to optimize development and production schemes, it is vital to know the dimensions and orientation of each sandstone body. Although the sedimentary facies and the orientation of paralic sand bodies have been extensively studied, there is little quantitative data on sand-body dimensions. This paper addresses that data gap and reports an extensive database of widths, lengths, and thicknesses of paralic sandstones.

Following an approach that has been successful in fluvial successions, an attempt is made to develop predictive relationships between sand-body thickness, which is commonly known from well data, and the key unknowns of width and sand-body length. In pursuing this goal, in addition to classifying the data by sand-body type, grain size, basin type, etc., a key aim of this study has been to test the hypothesis that sand-body dimensions are controlled by their sequence-stratigraphic setting.

Crossplots of sand-body width against thickness show that discrimination of the data by sand-body type produces the tightest set of clusters; therefore, this should be the first step in choosing a realistic range of dimensions for a given sandstone thickness. Further analysis reveals that sequence stratigraphic setting is a useful means of refining the choice of analog and reducing the range of dimensions.

Specific conclusions are (1) Valleys are much wider than channels. Crude averages show that channels (distributary channels, crevasse channels, etc.) are narrow, less than 1 km in width, with aspect ratios of 1:100, whereas valleys average

around 10 km in width and have aspect ratios on the order of 1:1000. (2) Shoreline-shelf sands are huge sheets tens to hundreds of kilometers in length, with mean widths that range from 7 to 25 km and vary according to systems tract. Shoreline-shelf sands deposited in highstand systems tracts are, on average, twice as wide as those deposited in transgressive systems tracts. Thicknesses of shoreline-shelf sands relate strongly to their position within a sequence set. (3) Valleys and shoreline-shelf sands have areal extents comparable to giant oil fields. Flood tidal deltas and mouth bars are comparable in area to small fields. (4) Distributary channels, crevasse channels, tidal flats, and crevasse splays are small areally. (5) Some systematic trends occur (e.g., in flood tidal deltas), allowing the prediction of width and length from thickness. Other data sets show a high degree of scatter, but maximum, mean, and minimum values can be determined for width, length, and thickness. (6) There is a clear partitioning of certain sand-body types into certain systems tracts.

INTRODUCTION

The scale, geometry, and orientation of reservoir sandstone bodies are critical in appraising, developing, and producing petroleum reservoirs. For example, an exploration well in a paralic succession may encounter petroleum in a series of stacked reservoirs. Seismic data can usually give a reliable estimate of structural closure, but how extensive will the reservoirs be? Will they be field-wide or will they cover only part of the closure, and what chance is there of other sands of limited lateral extent being present but not having been contacted by the discovery well (Figure 1)?

In some cases, careful horizon-slicing of high-quality, three-dimensional (3-D) seismic data sets can directly image reservoir sands, so that these questions can be answered rapidly and with a low degree of uncertainty (e.g., Flint et al., 1988). In many other examples, 3-D seismic data are either not available or they lack sufficient resolution to image individual sandstones (as is commonly the case in the Brent province) (e.g., Williams and Milne, 1991).

©Copyright 1999. The American Association of Petroleum Geologists. All rights reserved.

¹Manuscript received August 11, 1997; revised manuscript received June 16, 1998; final acceptance July 14, 1998.

²BP Exploration, BP Plaza, Westlake Park Boulevard, Houston, Texas 77079; e-mail: reynoldt@bp.com

I am grateful to BP Exploration for permission to publish this paper. Thanks are also extended to AAPG reviewers Lesley W. Evans, J. R. J. Studlick, and G. J. Moir, and to numerous colleagues, in particular Mike Mayall and Mark Eller, whose comments significantly improved this paper.

The data presented here can be used in three main ways: (1) as input to stochastic modeling packages to constrain the likely dimensions of sand bodies that cannot be correlated deterministically across a field, (2) to aid deterministic correlations by suggesting which sands are likely to be field wide, and (3) to suggest how sand-body dimensions vary systematically with sequence stratigraphic architecture.

DATABASE AND METHODOLOGY

Data Collection

The paper reports a study of 671 paralic sandstone bodies. Data were collected from examples in the published literature and collated from studies commissioned by British Petroleum. To speed data collection, and for compatibility with reported studies, maximum thicknesses, maximum widths, and maximum lengths were measured (Figure 2). The data are drawn entirely from ancient successions. An alternative approach of using aerial and satellite photographs to study modern deposits was not employed because of the difficulty of making a connection between the areal extent of present-day environments (e.g., channel width) and preserved sediment body geometries, and because aerial photographs yield little or no data on sand-body thickness.

Along with other workers (notably Bryant and Flint, 1993), it was thought the changes in base level and sediment supply that are highlighted by sequence stratigraphic studies would have a considerable influence on the dimensions of paralic sandstone bodies. To that end, the dimensional data were recorded in a sequence stratigraphic framework. Table 2 shows the sequence stratigraphic hierarchy that was employed, together with the full range of data that were recorded, only some of which are reported here.

Although the data collection process is generally satisfactory, several potential pitfalls need to be addressed.

Maximum Thicknesses

The thickness of sand bodies varies spatially. Maximum thickness is the quickest, but only one of a number of possible measurements that could be made to capture this variability. Hirst et al. (1993) argued persuasively that any individual well bore is unlikely to penetrate the maximum thickness of a fluvial channel sand body because the thickness of a sand body will vary both across its width and downstream from riffle to pool. They suggested instead that a well bore is more likely to encounter an average channel thickness that is typically between 0.6 and 0.8 of the maximum channel

thickness (Figure 2C). This logic can be extended to a wide range of sand-body types, and, therefore, well-bore thicknesses may need a correction before using maximum thickness crossplots to predict widths or lengths. The degree of required correction is likely to vary between depositional environments, with more correction needed in channelized sand bodies, but less correction needed where sandstones have a sheet geometry.

Tectonics

In tectonically active basins the extent, geometry, and orientation of sandstone bodies are commonly influenced by tectonic lineaments (Mitchell and Reading, 1986). The sand-body dimensions presented here are taken from basins that are dominated by regional subsidence and lack local synsedimentary faulting; therefore, the data are not thought to be influenced by local tectonics, but rather by a combination of regional base-level changes, sediment supply, and sedimentary processes.

Stacked Sand Bodies

As far as possible the dimensions presented here are derived from individual, rather than stacked, sand bodies. The problem of stacked sand bodies is particularly clear from fluvial successions where both multistory and multilateral channel sand bodies occur (Figure 2D). By contrast, distributary channel sandstone bodies tend to be ribbon-like, reflecting the strongly distributive channel pattern that characterizes delta plain settings, and although the sand bodies may be multilateral they are rarely multistory (e.g., Dreyer, 1990; Dreyer et al., 1990; Flores et al., 1991; Olsen, 1993). Similarly, other types of sandstone bodies are rarely stacked or amalgamated when viewed at the parasequence scale; they are commonly separated by flooding surfaces or their equivalents. Flood tidal deltas are an exception as they are commonly amalgamated laterally (e.g., Barwis, 1990).

Interpretation

Assignment of sand bodies to different depositional environments and their classification in a sequence stratigraphic framework is an interpretational exercise. Different workers may have chosen interpretations that differ from those presented here. The majority of the interpretations and the raw data were provided by specially commissioned studies. The remainder were gleaned from the literature, which increasingly provides detailed dimensional data in a sequence stratigraphic framework (e.g., O'Byrne and Flint, 1993).

Table 2. Data Collected for Each Sand Body in the Database

Sequence Stratigraphic Setting	
Parasequence (name)	
Parasequence set (forestepping, backstepping, aggradational)	
Systems tract (highstand, lowstand, transgressive, shelf margin)	
Sequence (name)	
Sequence set (forestepping, backstepping, aggradational)	
Margin type (ramp, shelf-slope)	
Basin type (foreland, rift, passive margin, etc.)	
Other Data Reported in this Paper	
Maximum thickness	
Maximum width	
Maximum length	
Grain size	
Sand-body type	
Data Collected But Not Reported in this Paper	
Orientation	
Distance to nearest sand body (to the left, right, above, and below)	
Nearest sand-body type	
Relative influence of sedimentary process: fluvial, storm, wave, tide	
Delta type: shelf edge or shelf delta	
Environment and subenvironment	
Paleolatitude and paleolongitude	
Age	
Data type	
Data quality	

sandstone body types. By contrast, similar plots (not presented here) of paralic sandstone bodies differentiated solely by systems tract, grain size, and basin type do not reveal distinct clusters.

As a result, recognizing sand-body type is the first step in choosing a set of analog dimensional data. The relatively restricted thickness range of paralic sandstones is thought to reflect the generation of accommodation space in relatively thin and uniform increments. Consider, for example, autocyclic lobe switching on a delta. An abandoned lobe is transgressed and subsides. Eventually, the active distributary system switches back and progrades a shelf delta over the old abandoned lobe. During progradation the delta may deposit a number of sandstone bodies of varying width and length, reflecting the size of the fluvial system and depositional processes (waves, tides, crevassing, etc.). However, none of the sand bodies are likely to be thicker than the amount of accommodation space generated during transgression and subsidence prior to delta switching, sediment supply, and renewed progradation. Valleys are a lone exception to this rule. Valleys erode down as far as

base-level fall permits, and form by far the thickest paralic sandstone bodies (Table 3).

Valleys and Channels

Cumulative frequency plots show that valleys and channels have dramatically different widths. Approximately 95% of distributary channels have widths less than 2 km, whereas 95% of the valleys have widths greater than 2 km (Figure 5). Channels range from tens of meters to 6 km in width; valleys range from 0.5 to over 60 km in width (Figure 6).

Channels have average widths of less than 1 km and aspect ratios (i.e., thickness:width ratios) of around 1:100. By contrast, valleys have an average width around 10 km and aspect ratios of 1:1000 or more (Table 3). Considerable overlap exists in the thicknesses of valleys and channels, and, in addition, they have similar log expressions (e.g., Eschard et al., 1991). However, valleys are generally wider than channels, and it is critical to distinguish them.

An analysis of the valley data alone reveals two trends (Figure 7). The first trend comprises a set of deep, narrow valleys with aspect ratios of around 1:100. All of these valleys have siltstone fills and incise into a distinct shelf-slope break. The second trend comprises relatively wide, shallow valleys that have aspect ratios of 1:1000, sandy fills, and developed on low-angle clastic ramps or far away from a coeval shelf-slope break. One possibility to explain these two trends is that the deep, narrow valleys with silty fills originated in a manner suggested by the flume experiments of Wood et al. (1993). These workers showed how base-level fall below the shelf edge can result in numerous local incisions, only one of which (eventually) links with the preexisting fluvial system. The other incisions are filled by material either (1) derived locally from reworking the shelf-slope break, and/or (2) derived from hemipelagic fallout during transgression. Such fills are likely to be silty. Alternatively, Schuam (1993) suggested that valley width relates to the rate of base-level fall and to the cohesion of the substrate, with rapid base-level fall and cohesive substrates favoring narrow, deep valleys.

Channels

A series of plots differentiating channels by channel type (Figure 6) and by systems tract and grain size (Figure 8) reveals that channel type is the best way of differentiating the range of channel dimensions into clustered subgroups. Crevasse channels are the narrowest and most shallow; distributary channels are the widest and deepest (Figure 6;

